

Canonical methods of constructing invariant tori by phase-space sampling

Teemu Laakso^{a,*}, Mikko Kaasalainen^a

^a*Department of Mathematics, Tampere University of Technology, PO Box 553, 33101 Tampere, Finland*

Abstract

Invariant tori in phase space can be constructed via a nonperturbative canonical transformation applied to a known integrable Hamiltonian \mathcal{H} . Hitherto, this process has been carried through with \mathcal{H} corresponding to the isochrone potential and the harmonic oscillator. In this paper, we expand the applicability regime of the torus construction method by demonstrating that \mathcal{H} can be based on a Stäckel potential, the most general known form of an integrable potential. Also, we present a simple scheme, based on phase space sampling, for recovering the angle variables on the constructed torus. Numerical examples involving axisymmetric galactic potentials are given.

Keywords: near integrability, invariant torus, torus construction, galaxies, Stackel potential

2010 MSC: 70H07, 70H15, 70K43, 65P10, 85A05

1. Introduction

Poincaré called the problem of determining the dynamical behaviour of a system given by a perturbed integrable Hamiltonian “the fundamental problem of dynamics”. He was quite right in doing so, as the problem has indeed proven to be one of the cornerstones of modern dynamics. The inverse version of this problem, though just as interesting, has attracted less attention. One reason for this is that, as befits an inverse problem, it is quite challenging and without a unique solution. Both problems can be expressed by the fundamental equation

$$H(\theta, J) = H_0(J) + \epsilon H_1(\theta, J),$$

where $H_0 : \mathbb{R}^n \rightarrow \mathbb{R}$ is an integrable Hamiltonian, $H, H_1 : \mathbb{R}^{2n} \rightarrow \mathbb{R}$ are general Hamiltonians, $\theta \in \mathbb{R}^n$, $J \in \mathbb{R}^n$ are action-angle variables corresponding to H_0 , and ϵ is a (small) constant. In the direct problem, H_0 and ϵH_1 are known, while in the inverse one we know an H in the form $H(p, q)$, where $p \in \mathbb{R}^n$, $q \in \mathbb{R}^n$ are some canonically conjugate coordinates, and want to find an H_0 and its J (and the corresponding θ) such that ϵH_1 is as small as possible (in some sense). In other words, we want to find the integrable Hamiltonian H_0 best approximating

a given, typically near-integrable, Hamiltonian H . The key to this problem lies in the explicit construction of the suitable phase-space tori, labelled by J , with which H_0 can be defined [1, 2].

The general problem of torus construction must be approached nonperturbatively, as by definition we do not know any tori that could be perturbed KAM-like into some other suitable invariant tori. Such a route was taken by McGill and Binney [3], who presented a method (canonical torus modelling), where a model torus is defined by applying a canonical transformation in the form of a Fourier series to an integrable toy Hamiltonian \mathcal{H} . The model is fitted to a sample of phase-space points in such a way that it reconstructs any existing KAM tori of the given target Hamiltonian H , or creates invariant tori of some H_0 mimicking the properties of H in phase-space regions where H has no tori of its own. Ideally, $H_0 = H$ on all KAM tori of H . As shown by Kaasalainen [4, 5] the method can be applied even in chaotic or strongly resonant regions of the target phase-space.

In a wider scope, finding invariant structures in near-integrable systems is a problem of theoretical interest, but also encountered in many physical applications. Lan et al. [6] provide a useful list of references related to the topic. Numerical methods based on Fourier series are used to study particle physics [7], superconductivity [8], quantum dynam-

*Corresponding author

Email address: teemu.laakso@tut.fi (Teemu Laakso)

ics [9], celestial mechanics [10], etc. Often, these kinds of methods are general in nature, and many are also introduced as such [6, 11].

The canonical torus modelling must be specially tuned for each pair of \mathcal{H} and H . McGill and Binney [3] and Kaasalainen and Binney [12, 1] demonstrated the method in gravitational systems by using the analytically integrable potentials of the harmonic oscillator and the isochrone for \mathcal{H} . Here we present a natural continuation of this approach by employing Stäckel potentials, the widest category of known integrable systems whose Hamilton-Jacobi equation is explicitly separable, in our \mathcal{H} . Another, more application-dependent reason for using Stäckel potentials is that they produce the same topologically different orbit families that are typically found in large gravitationally bound systems. Thus one does not have to use different \mathcal{H} for different orbit types. Moreover, elliptic Stäckel potentials resemble the potentials of such systems much more than the isochrone or the harmonic oscillator. This reduces the need for additional point transformations needed to twist the orbits inherent to \mathcal{H} into suitable shapes as in Kaasalainen and Binney [12, 1].

The useful and natural properties of Stäckel potentials make the algorithm low-maintenance, which is desirable in applications such as determining the potential of our Galaxy from astrophysical data [13]. Besides, we have the possibility of readily producing fully three-dimensional models for gravitational systems (triaxial galaxy models). In terms of computational cost, the advantages introduce some overhead: although separably computable in a closed form, the action-angle variables in a non-trivial Stäckel potential do not have analytical expressions, which has an impact on the complexity of the implementation.

As a step towards the goals above, we have developed the analytical and computational tools for constructing invariant tori from an axisymmetric ellipsoidal Stäckel toy Hamiltonian \mathcal{H} . A solid basis for such development is given by de Zeeuw [14]. He introduces the perfect ellipsoid, a triaxial galaxy model which produces a Stäckel potential, and recreates the major orbit families that Schwarzschild [15] found by numerically simulating an elliptical galaxy in dynamical equilibrium. In this paper, we implement H as an axisymmetric special case, the perfect oblate spheroid. This galaxy model was first discovered by Kuzmin [16]. There is only one orbit family, the short-axis tube.

In a specific numerical example, we construct invariant tori of an H_0 approximating the Hamiltonian H of the axisymmetric logarithmic potential.

A major benefit of torus modelling is that one can create a system of action-angle variables for H_0 . The angle variables on the model torus are not needed during the construction process. However, they can be recovered afterwards by various means: Binney and Kumar [17] derived a partial differential equation for the model angles, and solved it using discrete Fourier transforms. Kaasalainen and Binney [12] used a method based on orbit integration, and found it superior. However, integrated orbits may quickly stray off the model torus, if it happens to be in a chaotic region of H . Here we introduce a general technique of computing the model angles. It is simple and based on the same phase-space sampling as in the torus algorithm itself.

The paper is organized as follows. First, we outline the torus modelling algorithm, and the new method of obtaining the model angles. Next, we review the process of computing the action-angle variables of the perfect oblate spheroid, and discuss some aspects in the implementation. A numerical example follows, where we demonstrate the presented methods.

2. Torus modelling

Let $\mathcal{H} : \mathbb{R}^3 \times \mathbb{R}^3 \rightarrow \mathbb{R}$ be an integrable Hamiltonian. Suppose that the corresponding Hamilton-Jacobi equation separates in some canonical phase-space coordinates (q, p) . It follows that we can explicitly solve three integrals of motion $I \in \mathbb{R}^3$. These restrict the motion in the phase space to a subset $\mathcal{A} \subset \mathbb{R}^3 \times \mathbb{R}^3$ which, for periodic motion, is homeomorphic to a torus \mathbb{T}^3 . The natural coordinates on the torus are the action-angle variables (ϑ, \mathcal{J}) . We have a coordinate transformation $\mathcal{A} \rightarrow \mathcal{A}$,

$$(q, p) \leftrightarrow (\vartheta, \mathcal{J}). \quad (1)$$

Consider a canonical transformation, given by the generating function

$$F(\vartheta, J) = \vartheta \cdot J - i \sum_{k \in D} S_k(J) \exp(ik \cdot \vartheta),$$

where $D \subset \mathbb{Z}^3 \setminus \{0\}$ is a set of multi-indices (wave numbers), and $S_k \in \mathbb{C}$ are (Fourier) coefficients.

Explicitly,

$$\mathcal{J} = J + \sum_{k \in D} k S_k(J) \exp(ik \cdot \vartheta), \quad (2)$$

$$\theta = \vartheta - i \sum_{k \in D} \frac{\partial S_k(J)}{\partial J} \exp(ik \cdot \vartheta). \quad (3)$$

The map $\mathcal{A} \rightarrow \mathcal{A}$,

$$(\vartheta, \mathcal{J}) \leftrightarrow (\theta, J),$$

establishes new phase space coordinates (θ, J) which we identify as action-angle variables; not those of \mathcal{H} , but some other integrable Hamiltonian H_0 .

Let $\mathcal{T} \subset \mathbb{R}^3 \times \mathbb{R}^3$ be a subset of phase space where J is constant. \mathcal{T} is homeomorphic to \mathbb{T}^3 , and we call it the model torus. Through the coordinate transformation $\mathcal{T} \rightarrow \mathcal{T}$,

$$(\theta, J) \leftrightarrow (q, p), \quad (4)$$

we define (θ, J) as action-angle variables of an integrable Hamiltonian H_0 which restricts the motion to \mathcal{T} .

In torus modelling, the idea is to choose the coefficients S_k , $k \in D$ in such a way that the model torus \mathcal{T} becomes an invariant torus of an H_0 close to the given target Hamiltonian $H : \mathbb{R}^3 \times \mathbb{R}^3 \rightarrow \mathbb{R}$ and identical to it on its existing KAM tori. This is achieved by studying H through the map $\mathcal{T} \rightarrow \mathbb{R} :$

$$(\vartheta, J) \mapsto (\vartheta, \mathcal{J}) \mapsto (q, p) \mapsto H(q, p)$$

which is independent of $\partial S_k / \partial J$ (the coefficients in Eq. (3)). An algorithm is introduced, as follows. First, we choose the value of J , and a grid of points $\vartheta_{(m)}$, $m = 1, \dots, M$ in the toy angle space. On the grid, we minimize

$$\chi^2 = \sum_{m=1}^M [H(\vartheta_{(m)}, J) - \bar{H}]^2, \quad (5)$$

where \bar{H} is the arithmetic mean of H over the grid;

$$\bar{H} = \frac{1}{M} \sum_{m=1}^M H(\vartheta_{(m)}, J).$$

After the minimization we have, on the model torus, $H(\vartheta, J) \approx H_0(J) := \bar{H}$, which means that the model torus \mathcal{T} , defined by J and $S_k(J)$, $k \in D$, either approximates an existing invariant torus of

H or creates a close equivalent in some region of phase space.

The domain of the angle variables ϑ is trivially $[0, 2\pi)^3$. The image of the map $(\vartheta, J) \leftrightarrow (q, p)$ is the model torus \mathcal{T} . Hence, at this point, we can access \mathcal{T} as a geometrical object in the phase space without using (3). We can, e.g., plot its Poincaré sections.

3. Model angles by phase-space sampling

The model angles θ were not needed in the torus algorithm above. However, in order to complete the set of variables (θ, J) on the model torus \mathcal{T} , and to use the map (4) explicitly, one needs to find values for the coefficients $\partial S_k / \partial J$.

Suppose that we have found coefficients S_k in such a way that J corresponds to a suitable invariant torus of $H_0 \approx H$. On this torus, the model frequencies are

$$\omega = \frac{\partial H}{\partial J}.$$

By denoting $u := (q, p)$, $u \in \mathbb{R}^3 \times \mathbb{R}^3$, we have, for a fixed value of ϑ ,

$$\omega = \frac{\partial H}{\partial u} \frac{\partial u}{\partial \mathcal{J}} \frac{\partial \mathcal{J}}{\partial J}, \quad (6)$$

where $\partial u / \partial \mathcal{J}$ is a 6×3 matrix, $\partial \mathcal{J} / \partial J$ has 3×3 elements:

$$\frac{\partial \mathcal{J}}{\partial J} = I + \sum_{k \in D} \left[k \frac{\partial S_k}{\partial J} \right] \exp(ik \cdot \vartheta),$$

and I is a 3×3 identity matrix. The 3×3 matrix $[k \partial S_k / \partial J]$ is formed by the outer product of k and $\partial S_k / \partial J$:

$$\left[k \frac{\partial S_k}{\partial J} \right]_{ij} = k_i \frac{\partial S_k}{\partial J_j}.$$

Substituting, and considering each component ω_n , $n = 1, 2, 3$ separately, we have

$$\omega_n - \frac{\partial H}{\partial u} \frac{\partial u}{\partial \mathcal{J}} \sum_{k \in D} k \frac{\partial S_k}{\partial J_n} \exp(ik \cdot \vartheta) = \frac{\partial H}{\partial u} \frac{\partial u}{\partial \mathcal{J}_n}$$

which is a linear equation for the variables ω_n and $\partial S_k / \partial J_n$, $k \in D$. Since

$$\frac{\partial H}{\partial S_k} = \frac{\partial H}{\partial u} \frac{\partial u}{\partial \mathcal{J}} k \exp(ik \cdot \vartheta), \quad (7)$$

we can also write this as

$$\omega_n - \sum_{k \in D} \frac{\partial H}{\partial S_k} \frac{\partial S_k}{\partial J_n} = \frac{\partial H}{\partial u} \frac{\partial u}{\partial \mathcal{J}_n}. \quad (8)$$

Let $S \in \mathbb{C}^{\#D}$ be a vector which contains all of the coefficients S_k , $k \in D$. By dictating that Eq. (8) should hold on a grid of angles $\vartheta_{(m)}$, $m = 1, \dots, M$, we obtain a linear system $X\beta = y$, where each row X_m of X has the length $\#D + 1$;

$$X_m = \left[1 \quad - \frac{\partial H}{\partial S} \Big|_{J, \vartheta_{(m)}} \right],$$

$$\beta = \left[\omega_n \quad \frac{\partial S}{\partial J_n} \right]^T,$$

and the components y_m of y are

$$y_m = \frac{\partial H}{\partial u} \frac{\partial u}{\partial J_n} \Big|_{J, \vartheta_{(m)}}$$

The least-squares solution for β is given by the normal equations

$$X^T X \beta = X^T y. \quad (9)$$

The defined values of H_0 and ω on the constructed tori are self-consistent since $H_0 \equiv \bar{H} \implies \omega = \partial H_0 / \partial J = \partial \bar{H} / \partial \bar{J}$.

4. Oblate spheroidal Stäckel potentials

Ellipsoidal systems are most naturally represented in ellipsoidal coordinates. Adopting the notation of de Zeeuw [14], we define the triaxial ellipsoidal coordinates as the roots $\tau = \lambda, \mu, \nu$ of

$$\frac{x^2}{\tau + \alpha} + \frac{y^2}{\tau + \beta} + \frac{z^2}{\tau + \gamma} = 1,$$

where x, y, z are the Cartesian coordinates in \mathbb{R}^3 , and $\alpha, \beta, \gamma \in \mathbb{R}$ are coordinate parameters. Suppose that the parameters are selected in such a way that the coordinate surfaces match the geometry of the modelled system. When the model changes from triaxial to oblate spheroidal (axisymmetric with respect to z -axis), coordinates become the prolate spheroidal coordinates λ, ϕ, ν . Two of these are the roots $\tau = \lambda, \nu$ of

$$\frac{R^2}{\tau + \alpha} + \frac{z^2}{\tau + \gamma} = 1,$$

where $R^2 = x^2 + y^2$. The coordinates λ, ν are elliptical coordinates in the meridional plane the orientation of which is labelled by the azimuthal angle ϕ . The prolate spheroidal coordinates can also be represented by trigonometric functions, but in order to

ease the future transition to fully triaxial models, we adopt the definition above.

If we set $\alpha < \gamma$, and choose $\lambda > \nu$, we have $(\lambda, \nu) \in [-\alpha, \infty) \times [-\gamma, -\alpha]$. We select $\phi \in [0, \pi/2)$, and introduce an additional discrete variable $n \in \{-1, 1\}^3$ which identifies the octants in \mathbb{R}^3 . Let R, φ, z be the standard cylindrical coordinates. For the set of points $\mathbb{R}^3 \setminus \{R = 0\}$ we have a one-to-one correspondence:

$$(x, y, z) \leftrightarrow (R, \varphi, z) \leftrightarrow (\lambda, \phi, \nu, n).$$

An example of the prolate spheroidal coordinate surfaces is shown in Fig. 1. Surfaces of constant λ and ν are axisymmetric ellipsoids and hyperboloids, respectively.

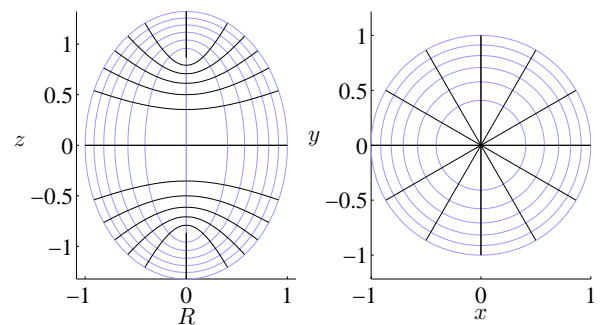


Figure 1: (Colour online) Prolate spheroidal coordinate surfaces ($\alpha = -1$, $\gamma = -0.25$) in the meridional (left) and equatorial (right) planes.

Consider an axisymmetric potential $\Psi : \mathbb{R}^2 \rightarrow \mathbb{R}$, $(\lambda, \nu) \mapsto \Psi(\lambda, \nu)$ in the prolate spheroidal coordinates. The Hamiltonian $\mathcal{H} : \mathbb{R}^2 \times \mathbb{R}^3 \rightarrow \mathbb{R}$ which describes the motion in Ψ satisfies $\mathcal{H}(\lambda, \nu, p_\lambda, p_\phi, p_\nu) = E$, where p_τ are the conjugate momenta to $\tau = \lambda, \phi, \nu$, and E is the constant energy (per unit mass). Due to axisymmetry, the z -component of the angular momentum is also constant, and our system could be reduced to planar. However, again, for the sake of future expandability, we treat the model as three-dimensional.

The Hamilton-Jacobi equation for \mathcal{H} is

$$\sum_{\tau} \frac{1}{2h_{\tau}^2} \left(\frac{\partial W}{\partial \tau} \right)^2 + \Psi - E = 0, \quad (10)$$

where the sum is taken over $\tau = \lambda, \phi, \nu$, and h_{τ} are the scale factors of the prolate spheroidal coordinates. The unknown function $W : \mathbb{R}^3 \rightarrow \mathbb{R}$, $(\lambda, \phi, \nu) \mapsto W(\lambda, \phi, \nu)$ is Hamilton's characteristic function.

By definition, the Hamilton-Jacobi equation for a Stäckel potential is separable. In prolate spheroidal coordinates such a potential can be written as

$$\Psi(\lambda, \nu) = -\frac{f_\lambda(\lambda) - f_\nu(\nu)}{\lambda - \nu}, \quad (11)$$

where f_λ and f_ν are arbitrary smooth real-valued functions. Solving Eq. (10) with (11) yields

$$W(\lambda, \phi, \nu) = \sum_{\tau} W_{\tau}(\tau),$$

where $W_{\tau} : \mathbb{R} \rightarrow \mathbb{R}$, and $\tau = \lambda, \phi, \nu$. There are two independent separation constants which, in addition to the total energy, translate to three integrals of motion; \mathcal{H} , I_2 , and I_3 .

If we interpret the constants $I = (\mathcal{H}, I_2, I_3)$ as new canonical momenta, $W(\lambda, \phi, \nu, \mathcal{H}, I_2, I_3)$ acts as a generating function which defines a canonical transformation; we have $p_{\tau} = \partial W / \partial \tau$ for $\tau = \lambda, \phi, \nu$, and the conjugate coordinates to I are $\partial W / \partial I$.

Suppose that the motion is quasiperiodic. The action integrals $\mathcal{J} = (\mathcal{J}_\lambda, \mathcal{J}_\phi, \mathcal{J}_\nu)$ are defined as

$$\mathcal{J}_{\tau} = \frac{1}{2\pi} \oint p_{\tau}(\tau', I) d\tau',$$

where the closed path integral is taken over a complete period of motion in the corresponding direction $\tau = \lambda, \phi, \nu$. The conjugate angles $\vartheta = (\vartheta_\lambda, \vartheta_\phi, \vartheta_\nu)$ are

$$\vartheta_{\tau} = \frac{\partial W}{\partial \mathcal{J}_{\tau}} = \frac{\partial W}{\partial I} \frac{\partial I}{\partial \mathcal{J}_{\tau}},$$

for each $\tau = \lambda, \phi, \nu$.

5. Algorithmic details

A detailed description, including explicit formulas and derivations, of using oblate spheroidal Stäckel toy Hamiltonians in torus modelling is given in Laakso [18]. Here, we give an overview, and focus on some essential points.

For an oblate spheroidal Stäckel Hamiltonian, equations above outline the explicit steps in the coordinate transformation (1), from left to right. The integrals of motion I can be solved algebraically, but numerical methods are required in various other places. First of all, we need one-dimensional root-finding algorithms in order to define the boundaries of the set \mathcal{T} in the prolate spheroidal coordinates

($p_{\tau}^2(\tau, I) \geq 0, \tau = \lambda, \nu$). For $\partial W / \partial I$ and \mathcal{J} we need to solve partly improper integrals with numerical quadrature rules. When (1) is implemented from right to left, (λ, ϕ, ν, n) and I are evaluated using multi-dimensional root-finding algorithms.

Although the prolate spheroidal coordinates $\tau = \lambda, \phi, \nu$ are suitable for numerical work, their conjugate momenta p_{τ} (or coordinate velocities $\dot{\tau}$) are not; points in the equatorial plane $\nu = -\gamma$ are singular in coordinate transformations, and in partial derivatives with respect to p_{ν} . Fortunately, these singularities can be avoided by manipulating equations with the polar coordinates $u := (R, \varphi, z, p_R, p_{\varphi}, p_z)$ as the frame of reference in phase space.

Additional numerical quadratures are needed in torus modelling, if we minimize the r.h.s. of Eq. (5) using gradient-based methods. We have to evaluate the partial derivatives $\partial H / \partial S_k$, and especially the matrix $\partial u / \partial \mathcal{J}$, as Eq. (7) suggests. The same partial derivatives are also needed when solving the model angles from Eq. (8). We obtain $\partial u / \partial \mathcal{J}$ by inverting $\partial(\vartheta, \mathcal{J}) / \partial u$. Especially the computation of $\partial \vartheta / \partial u$ is a nontrivial exercise.

Terms in the Fourier series (2) and (3) can be simplified or cancelled out, if the target Hamiltonian H shares some of the symmetries of H . We shall use a target which is time reversible, and symmetric about $R = 0$ and $z = 0$. This implies that each $S_k(J) = S_k(J_\lambda, J_\nu) \in \mathbb{R}$. The transformations (2) and (3) become

$$\mathcal{J} = J + 2 \sum_{k \in D_{\lambda\nu}^+} k S_k(J_\lambda, J_\nu) \cos(k \cdot \vartheta), \quad (12)$$

$$\theta = \vartheta + 2 \sum_{k \in D_{\lambda\nu}^+} \frac{\partial S_k(J_\lambda, J_\nu)}{\partial J} \sin(k \cdot \vartheta), \quad (13)$$

where the set $D_{\lambda\nu}^+$ is obtained from $D_{\lambda\nu} = \{(k_\lambda, k_\phi, k_\nu) \in \mathbb{Z}^3 \setminus \{0\} : k_\phi = 0\}$ by removing one of the two elements $k \in D_{\lambda\nu}$ for which $k = -k$. We have $\mathcal{J}_\phi = J_\phi$ and $\theta_\phi = \vartheta_\phi$.

6. Numerical examples

We use the perfect oblate spheroid as the toy potential in the torus algorithm. The arbitrary functions in the Stäckel potential (11) are thus

$$f_{\tau}(\tau) = -2\pi G \rho_0 \alpha \sqrt{-\gamma(\tau + \gamma)} \arctan \sqrt{\frac{\tau + \gamma}{-\gamma}},$$

for $\tau = \lambda, \nu$. G is the gravitational constant, and ρ_0 is the density at the origin. We set $G = 1$.

For the target Hamiltonian, we use the logarithmic potential in the meridional plane:

$$\Phi(R, z) = \frac{1}{2} \ln \left(R^2 + \frac{z^2}{a^2} + b^2 \right),$$

where $a = 0.8$ and $b = 0.14$. Thus $H = |p|^2/2 + \Phi$, where p is the momentum vector.

Before running the actual torus modelling algorithm, values for the parameters α , γ , and ρ_0 are chosen in such a way that the toy and target potential surfaces are as similar as possible in configuration space. We formulate this as a curve fitting problem which we solve in a sparse grid of points using the Levenberg-Marquardt algorithm. As a result, we have $\alpha = -0.639$, $\gamma = -0.142$, and $\rho_0 = 1.29$.

As an example, we ran the torus modelling algorithm for $J = (0.5, 0.45, 0.5) =: J_0$. The included number of Fourier coefficients S_k , $k \in D_{\lambda, \nu}^+$ was determined by trial and error. We found out that reasonable accuracy was achieved by including terms for which $|k_\lambda| \leq 96$ and $|k_\nu| \leq 24$. The toy angle grid was chosen to contain 100×100 points, which exceeds the Nyquist rate of the Fourier series.

The χ^2 minimization with Levenberg-Marquardt converged within a few steps; the magnitudes of the resulting Fourier coefficients are displayed in Fig. 2. In this case, the Fourier series converges for \mathcal{J}_λ

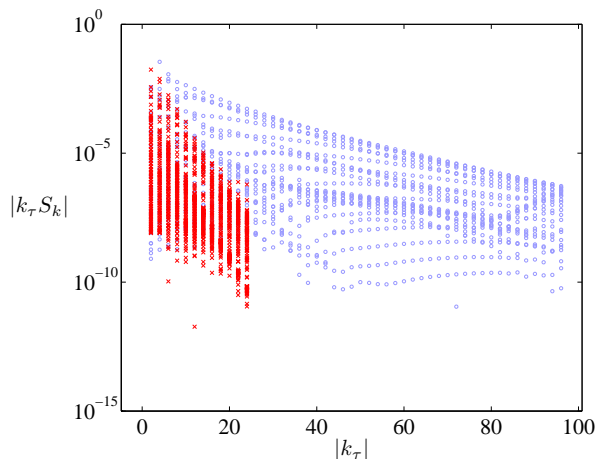


Figure 2: (Colour online) Magnitudes of the torus coefficients. Terms $|k_\lambda S_k|$ are plotted with light blue circles, and the terms $|k_\nu S_k|$ with red crosses.

about five times more slowly than for \mathcal{J}_ν .

Since axisymmetric systems are effectively two-dimensional, we may evaluate our success in torus modelling by plotting Poincaré sections. In Fig. 3 we have the section $z = 0$, $p_z > 0$, computed with the initial, unoptimized coefficients $S_k = 0$, $\forall k$. There are 16 discrete points, computed by choosing a grid in R , and solving for \dot{R} on the model torus $J = \mathcal{J}$. From each of these points an orbit in the target Hamiltonian H is integrated, and superimposed in the figure. Prior to the χ^2 minimization,

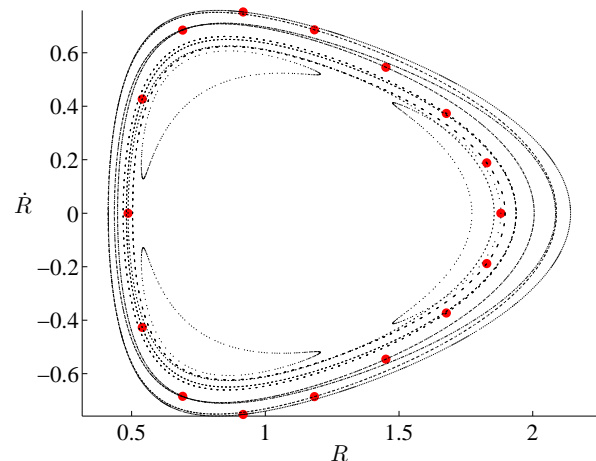


Figure 3: (Colour online) Initial ($S_k = 0$, $\forall k$) Poincaré section $z = 0$, $p_z > 0$ for the model torus (big red dots), and for superimposed trajectories in the target Hamiltonian H (small black dots).

the orbits clearly do not stay on the model torus. Figure 4 shows how the situation changes after optimization. Within observable accuracy, the integrated orbits now coincide with the model torus J .

As a more quantitative indicator of accuracy, we compute the time evolution of J along the integrated target orbits. In Fig. 5, for each orbit, we have plotted the change $\Delta J(t) = J(t) - J_0$, where J is obtained from (12) by approximating $S_k(J) \approx S_k(J_0)$ on the target torus. The accuracy of the torus model seems consistent with the included coefficients (Fig. 2). A better fit would be achieved by using a longer Fourier series and a denser angle grid.

The model angles θ and frequencies ω were computed with the phase-space sampling technique. By reusing the toy angle grid from the χ^2 minimization, the matrix X in the normal equations (9) had a size of 1213×10000 . Numerical solution for β was obtained through LU-decomposition. Validity was checked by computing the change $\Delta\omega(t) =$

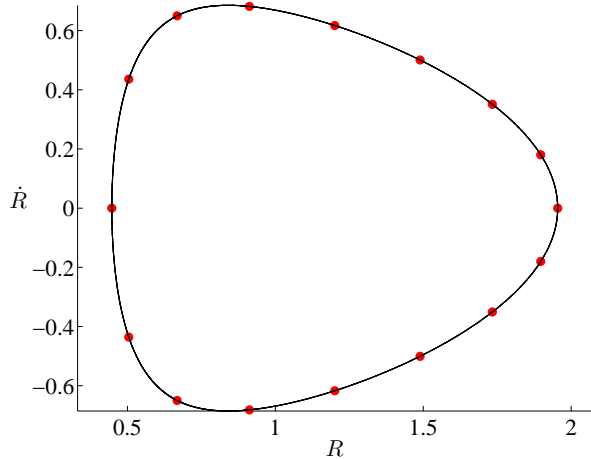


Figure 4: (Colour online) Final Poincaré section with optimized Fourier coefficients (cf. Fig. 3)

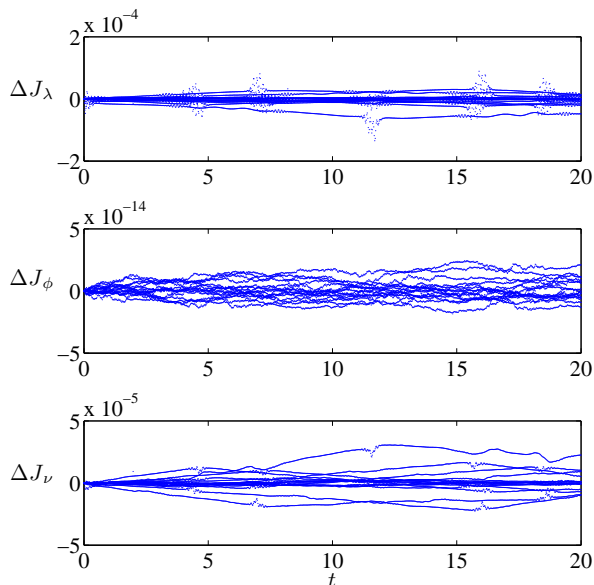


Figure 5: (Colour online) Changes in model actions J along target orbits. Each orbit is initially on the model torus J_0 (big red dots in Fig. 4).

$\omega(t) - \omega_0$, where ω_0 corresponds to J_0 , along the target orbits. This is shown in Fig. 6. The frequencies ω are computed from (6) using the approximation $\partial S_k(J)/\partial J \approx \partial S_k(J_0)/\partial J$ on the target torus. Since errors accumulate from two Fourier

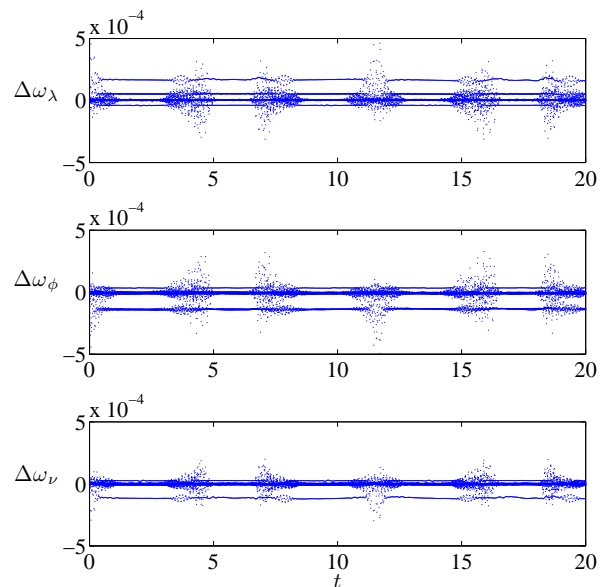


Figure 6: (Colour online) Changes in model frequencies ω along target orbits. Initial values as in Fig. 5.

series, the variation in ω is somewhat higher than the variation in J , but again, results are consistent, and show that, up to a reasonable accuracy, the obtained (θ, J) act numerically as the action-angle variables of an H_0 approximating H . The fuzzy parts of trajectories in Fig. 6 (and 5) correspond to phase-space regions, where the χ^2 minimization was least successful.

The numerical experiments above were repeated for several values of J . As a general rule, we found out that the Fourier series converged faster for thinner tori. On the other hand, arbitrarily thin tori could not be mapped by (2) because of the requirement $\mathcal{J} \geq 0$. When probing small values of J_λ with $J_\phi = 0.45$ and $J_\nu = 0.25$, the thinnest mappable torus was around $J_\lambda = 0.01$. For tori thicker than J_0 , more Fourier terms were required for maintaining a similar level of accuracy. In the comfortable region of the target actions J , the results were typically as good as in Fig. 2-6.

7. Discussion

We have demonstrated that an axisymmetric ellipsoidal Stäckel potential can be used for constructing invariant tori, and associated action-angle variables, for an integrable approximation of an axisymmetric logarithmic potential. Similar targets should yield equally successful results, since the target effectively acts as a plug-in, and can be changed in the torus algorithm with a relatively small effort. The determination of the action-angle variables of the tori is based on phase-space sampling rather than orbit integration, making the procedure manifestly geometric in character.

In the examples above, within a comfortable range of the model actions, the convergence of the algorithm was excellent, but the suitable number of Fourier terms had to be sought by trial and error. We found out that for $\mathcal{J}_\lambda = \mathcal{J}_\nu$, considerably different amounts of terms were required in the λ and ν directions. Using an unbalanced number of Fourier terms is uneconomical, since the number of points in the ϑ -grid is chosen according to the highest frequency in the Fourier series. One possibility is to balance the situation by adjusting the toy potential (and coordinate) parameters during χ^2 optimization as in McGill and Binney [3] and Kaasalainen and Binney [12], although this increases the computational overhead somewhat.

The main advantage of modelling with Stäckel potentials, as opposed to the special analytically integrable ones; isochrone, harmonic oscillator, etc. is in their generality. They possess the ability to mimic the full range of orbital features. However, this freedom comes at a cost, since the Hamilton-Jacobi equation must be solved numerically, and the computation times for Stäckel models are considerably higher. In this paper, we have studied the perfect oblate spheroid which is a special case of the perfect ellipsoid. The success with the axisymmetric Stäckel potential paves way to future three-dimensional models accessible with a relatively straightforward expansion of our algorithm.

- [1] M. Kaasalainen, J. Binney, Construction of Invariant Tori and Integrable Hamiltonian, *Phys. Rev. Lett.* 73 (1994) 2377–2381.
- [2] J. Pöschel, Integrability of Hamiltonian systems on Cantor sets, *Comm. Pure Appl. Math.* 35 (1982) 653–695.
- [3] C. McGill, J. Binney, Torus construction in general gravitational potentials, *Mon. Not. R. Astron. Soc.* 240 (1990) 634–645.
- [4] M. Kaasalainen, Hamiltonian perturbation theory for

- numerically constructed phase-space tori, *Mon. Not. R. Astron. Soc.* 268 (1994) 1041–1050.
- [5] M. Kaasalainen, Construction of invariant tori in chaotic regions, *Phys. Rev. E* 52 (1995) 1193–1196.
- [6] Y. Lan, C. Chandre, P. Cvitanović, Newton’s descent method for the determination of invariant tori, *Phys. Rev. E* 74 (2006) 046206.
- [7] R. L. Warnock, Close Approximations to Invariant Tori in Nonlinear Mechanics, *Phys. Rev. Lett.* 66 (1991) 1803–1806.
- [8] V. López, P. Boyland, M. T. Heath, R. D. Moser, Relative periodic solutions of the complex Ginzburg-Landau equation, *SIAM J. Appl. Dyn. Syst.* 4 (2005) 1042–1075.
- [9] S. Gekle, J. Main, T. Bartsch, Torus Construction and Quantization for the Hydrogen Atom in Crossed Electric and Magnetic Fields, *Nonlinear Phenom. Complex Syst.* 10 (2007) 164–169.
- [10] E. Castella, À. Jorba, On the vertical families of two-dimensional tori near the triangular points of the bicircular problem, *Celest. Mech. Dyn. Ast.* 76 (2000) 35–54.
- [11] À. Jorba, M. Ollé, Invariant curves near Hamiltonian-Hopf bifurcations of four-dimensional symplectic maps, *Nonlinearity* 17 (2004) 691–710.
- [12] M. Kaasalainen, J. Binney, Torus construction in potentials supporting different orbit families, *Mon. Not. R. Astron. Soc.* 268 (1994) 1033–1040.
- [13] J. Binney, Modelling the Galaxy for Gaia, in: *The Three-Dimensional Universe with Gaia*, vol. 576 of *ESA Conference Proceedings*, 89–95, 2005.
- [14] T. de Zeeuw, Elliptical galaxies with separable potentials, *Mon. Not. R. Astron. Soc.* 216 (1985) 273–334.
- [15] M. Schwarzschild, A numerical model for a triaxial stellar system in dynamical equilibrium, *Astrophys. J.* 232 (1979) 236–247.
- [16] G. G. Kuzmin, A stationary galaxy model admitting triaxial velocity distribution, *Astron. Zh.* 33 (1956) 27–45.
- [17] J. Binney, S. Kumar, Angle variables for numerically fitted orbital tori, *Mon. Not. R. Astron. Soc.* 261 (1993) 584–592.
- [18] T. Laakso, Embracing Integrability in Stellar and Planetary Dynamics, Ph.D. thesis, University of Helsinki, <http://urn.fi/URN:ISBN:978-952-10-7161-4>, 2011.